

# Dendritic amplification of inhibitory postsynaptic potentials in a model Purkinje cell

Sergio M. G. Solinas, Reinoud Maex and Erik De Schutter

Laboratory of Theoretical Neurobiology, Institute Born-Bunge, University of Antwerp, Universiteitsplein 1, B-2610 Antwerpen, Belgium

**Keywords:** active membrane, cerebellum, dendritic tree, inhibitory postsynaptic potential, multicompartmental model

## Abstract

In neurons with large dendritic arbors, the postsynaptic potentials interact in a complex manner with active and passive membrane properties, causing not easily predictable transformations during the propagation from synapse to soma. Previous theoretical and experimental studies in both cerebellar Purkinje cells and neocortical pyramidal neurons have shown that voltage-dependent ion channels change the amplitude and time-course of postsynaptic potentials. We investigated the mechanisms involved in the propagation of inhibitory postsynaptic potentials (IPSPs) along active dendrites in a model of the Purkinje cell. The amplitude and time-course of IPSPs recorded at the soma were dependent on the synaptic distance from the soma, as predicted by passive cable theory. We show that the effect of distance on the amplitude and width of the IPSP was significantly reduced by the dendritic ion channels, whereas the rise time was not affected. Somatic IPSPs evoked by the activation of the most distal synapses were up to six times amplified owing to the presence of voltage-gated channels and the IPSP width became independent of the covered distance. A transient deactivation of the  $\text{Ca}^{2+}$  channels and the  $\text{Ca}^{2+}$ -dependent  $\text{K}^+$  channels, triggered by the hyperpolarization following activation of the inhibitory synapse, was found to be responsible for these dynamics. Nevertheless, the position of activated synapses had a marked effect on the Purkinje cell firing pattern, making stellate cells and basket cells most suitable for controlling the firing rate and spike timing, respectively, of their target Purkinje cells.

## Introduction

Information processing in the brain, as we understand it, is built upon the single-neuron input/output function (Koch & Segev, 2000). The neuronal output, the action potential, results from the integration of currents in the soma and initial axon segment. The input accesses the neuron primarily in the dendrite. Neuronal information processing takes place along the remaining path from synapse to soma. In small neurons the processing can be as straightforward as a temporal summation of the postsynaptic potentials. The input/output function becomes more complex in larger neurons in which huge numbers of synapses and voltage-dependent ion channels and a longer synapse-to-soma path make non-linear and prolonged interactions possible. Passive filtering within a large dendritic tree most profoundly attenuates the postsynaptic potentials triggered at distal synapses (Rall, 1970; Jack *et al.*, 1975). However, voltage-dependent ion channels may abolish the synaptic-location dependency of the somatic postsynaptic potentials by boosting the more distally generated currents, as demonstrated in models of excitatory synaptic input to neocortical or CA1 pyramidal neurons (Bernander *et al.*, 1994; Cook & Johnston, 1997; Williams & Stuart, 2003a) and cerebellar Purkinje cells (PCs) (De Schutter & Bower, 1994c; De Schutter & Steuber, 2000).

Similarly, voltage-dependent ion channels have been suggested to boost inhibitory postsynaptic potentials (IPSPs) in neocortical

pyramidal neurons (Williams & Stuart, 2003b) but it is not known if this also occurs in PCs. PCs receive extensive inhibition from stellate and basket cells, located at different depths within the molecular layer. Stellate cells target the richly arborized PC distal dendrite, whereas basket cells form axonal plexi at the level of the PC main dendrite, soma and initial axon segment (Palay & Chan-Palay, 1974; Sultan & Bower, 1998). As stellate cells can contact PC dendrites throughout the molecular layer (Häusser & Clark, 1997), the experimental investigation of the relationship between the location of the activated synapses and the amplitude and time-course of the somatically recorded IPSPs is more difficult in PCs than in cortical (Williams & Stuart, 2003b) or hippocampal (Miles *et al.*, 1996; Maccaferri *et al.*, 2000) pyramidal neurons.

Therefore, we investigated this issue in a detailed model of the cerebellar PC (De Schutter & Bower, 1994a,b). We simulated the amplification of IPSPs by voltage-dependent and  $\text{Ca}^{2+}$ -gated ion channels and the effect on the PC firing pattern produced by variations in the balance between dendritic and somatic inhibitory inputs.

## Materials and methods

### Model Purkinje cell

The present model PC is an updated version of the multicompartmental model published originally by De Schutter & Bower (1994a,b). The dendritic tree is a reconstruction of a guinea-pig PC (Rapp *et al.*, 1994), discretized into 4500 compartments and spines. The passive membrane had a specific capacitance of  $1.64 \mu\text{F}/\text{cm}^2$  and specific

Correspondence: Dr Sergio Solinas, as above.  
E-mail: sergio@tmb.ua.ac.be

Received 11 March 2005, revised 21 November 2005, accepted 21 November 2005

resistances of 10 k $\Omega$  cm<sup>2</sup> in the soma and 30 k $\Omega$  cm<sup>2</sup> in the dendrite, yielding an input resistance of 19.6 M $\Omega$  (De Schutter & Bower, 1994a).

#### Active membrane

The model had the following 10 voltage-gated and Ca<sup>2+</sup>-dependent conductances: an inactivating and a persistent Na<sup>+</sup> channel (restricted to the soma); P-type and T-type Ca<sup>2+</sup> channels; an anomalous inward rectifying channel producing the hyperpolarization-activated mixed cationic current ( $I_h$ ); a delayed-rectifier, a persistent and an A-type K<sup>+</sup> channel; a high-threshold Ca<sup>2+</sup>-activated K<sup>+</sup> channel of the BK type and a low-threshold Ca<sup>2+</sup>-gated K<sup>+</sup> channel of the K2 type. The original PC model did not have hyperpolarization-activated channels in its dendrite but instead a somatic  $I_h$  current accounted for the inward rectification observed in rat PCs (Crepel & Penit-Soria, 1986). As dendritic  $I_h$  currents were recently shown to significantly affect the time-course of excitatory postsynaptic potentials (EPSPs) (Roth & Häusser, 2001), we incorporated a new  $I_h$  in the PC model, uniformly distributed over the entire neuron. This non-inactivating  $I_h$  channel had first-order kinetics, as described by Roth & Häusser, 2001):

$$dh/dt = \alpha(1 - h) - \beta(h)$$

where  $\alpha = a/\exp[-b(V - V_{1/2})]$  and  $\beta = c/\exp[c(V - V_{1/2})]$ . The parameter values were  $a = 0.63$  s<sup>-1</sup>,  $b = 0.063$  mV<sup>-1</sup>,  $c = 0.079$  mV<sup>-1</sup> and  $V_{1/2} = -73.2$  mV. The channel density was 25  $\mu$ S/cm<sup>2</sup> and the reversal potential -30 mV. The other channels had the kinetics and densities of the PM9 model as described in De Schutter & Bower (1994a).

#### Synaptic kinetics

The model had 1474 AMPA receptor synapses located on dendritic spines and 1600 GABA<sub>A</sub> receptor synapses on compartments representing the shafts of thick and spiny dendrites. We matched the synaptic kinetics to recent data and adjusted the peak conductances so as to obtain simulated somatic EPSCs and IPSCs with amplitude distributions similar to those measured experimentally. In order to avoid mismatches due to an incomplete space clamp of the dendritic tree of actual PCs or to the low input resistance of the model PC, the unitary synaptic peak conductances needed to generate the experimental somatic excitatory and inhibitory current amplitudes were recalculated during simulated voltage clamp of the soma, using holding potentials of -70 mV (Barbour, 1993; Isope & Barbour, 2002) and -60 mV (Pouzat & Hestrin, 1997), respectively. For these simulations, the reversal potential of the GABAergic synapses was shifted to 0 mV to mimic the symmetric chloride concentration configuration. The resultant peak amplitude distributions of EPSCs and IPSCs are shown in Fig. 1. The parameter values were as follows. For the AMPA receptor synapses made by parallel fibres: peak conductance, 1.3 nS; rise and decay time constants, 0.6 and 1 ms; resultant mean amplitude of somatic EPSCs, 10 pA (Isope & Barbour, 2002). For the GABA<sub>A</sub> receptor synapses made by stellate cells: peak conductance, 2.9  $\pm$  2 nS (Jaeger *et al.*, 1997); rise and decay time constants, 1 and 5 ms; resultant mean amplitude of somatic IPSCs, 32 pA (Pouzat & Hestrin, 1997). [Note that the variability in the peak conductance of the GABA<sub>A</sub> receptor synapses reflects the variable size of the postsynaptic dendritic compartments (De Schutter & Bower, 1994b; Jaeger *et al.*, 1997). As spines had a fixed size in our model, no such variability existed for the parallel-fibre synapses.] The soma and main dendrite had GABA<sub>A</sub> receptor synapses which were activated by basket cells (Palay & Chan-Palay, 1974). Their rise and decay time

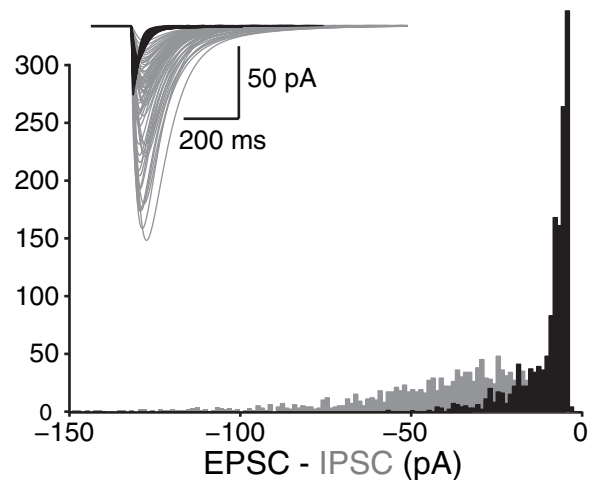


FIG. 1. The distribution of the somatic peak amplitude of all unitary excitatory (EPSCs, black) and inhibitory (IPSCs, gray) postsynaptic potentials in the model Purkinje cell, obtained from simulated voltage clamp of the soma. The inset shows examples of the injected clamp current. The IPSCs are inward because the reversal potential of the inhibitory synapses was set to 0 mV to mimic the effects of the high symmetric chloride concentration used by Pouzat & Hestrin (1997).

constants were set to 1 and 5 ms. The peak conductance was 3.5 nS for the somatic synapses and 3 nS for those on the main dendrite (Pouzat & Hestrin, 1997; Yoshida *et al.*, 2002).

We did not model the serotonin-driven GABAergic input from Lugaro cells (Dean *et al.*, 2003) or the inwardly rectifying K<sup>+</sup> current operated by GABA<sub>B</sub> receptors (Tabata *et al.*, 2005).

#### Synaptic activation

In all simulations, the synaptic channels were activated by independent random spike trains having a Poisson interval distribution, produced with a generalized Marsaglia-Fibonacci two-seed random-number generator (Marsaglia, 1985). The minimum interspike interval was 1 ms to mimic the absolute refractory period of the molecular layer interneurons and the granule cells (Isope & Barbour, 2002). From quantitative morphological data (Eccles, 1973; Harvey & Napper, 1991; Sultan & Bower, 1998), it can be derived that a single PC is innervated by approximately 150 interneurons (Solinas *et al.*, 2003). We therefore stimulated the inhibitory synapses of the model PC by a population of 150 random-spike generators, divided into stellate and basket cell subgroups. Each of the first subgroup of 105 random-number generators activated, on average, nine GABA<sub>A</sub> receptor synapses on spiny and thick dendrites, as stellate cells do (Jaeger *et al.*, 1997; Sultan & Bower, 1998). Each of the other subgroup of 45 random-spike generators activated a separate synapse located on the PC soma and main dendrite, modeling the basket cell input. Synaptic plasticity and probability of release were not modeled.

#### Simulation strategy

We simulated three versions of the model PC: a completely active PC model (aPC); a partially active model in which the voltage-gated channels of the soma were blocked [active dendrite PC model (adPC)] and a completely passive PC model (pPC). All simulations were run using the General Neural Simulation System GENESIS (Bower & Beeman, 1998).

The aPC was used to select proper background excitatory and inhibitory input rates so as to produce physiological firing patterns in the model (De Schutter & Bower, 1994b). When each excitatory synapse was activated with an input rate of 10 spikes/s and each stellate inhibitory synapse with a rate of 28 spikes/s (Armstrong & Rawson, 1979), the aPC fired irregularly at a frequency of 50 spikes/s and with a coefficient of variation (CV) of the interspike interval equal to 0.8. These same background input spike trains were used to drive all models, unless otherwise stated. Note that the PC model had only 1% of the number of excitatory synapses impinging on a real PC. Thus, delivering 10 spikes/s to each AMPA receptor yielded a mean depolarizing postsynaptic current equivalent to a total excitatory input delivered by 147 400 parallel fibres with an individual rate of 0.1 spikes/s. Recent experiments showed that cerebellar granule cells have an extremely low spontaneous firing rate *in vivo* (Chadderton *et al.*, 2004).

The pPC and adPC were simulated in order to examine the effect of active membrane channels on the propagation to the soma of distal IPSPs. We used three strategies to improve the signal-to-noise ratio and hence to reduce the number of stimulus repetitions. In a first set of simulations, we computed the compound IPSP (cIPSP) generated by the simultaneous activation of 42 synapses on a peripheral dendritic branch, simulating input from synchronized stellate cells. In a second set of simulations, we computed the unitary IPSPs generated by the stimulation of the synapses on a single compartment, simulating a dynamic-clamp experiment. Indeed, a PC receives multiple synaptic contacts from each stellate cell, which possibly project onto different dendritic branches (Sultan & Bower, 1998). Thus, the IPSP is spread over many branches making its peak amplitude dependent on the recording site. Dynamic-clamp experiments offer the advantage that the stimulation electrode delivers input to a restricted area of the dendrite only (Williams & Stuart, 2003b). Hence, to simulate IPSPs like those generated in a dynamic-clamp experiment, we made each stellate cell contact only one GABAergic synapse having its peak conductance set to 26.1 nS. Finally, in simulations run to examine the contribution of individual ion currents to the amplification mechanism, we eliminated the noise inherent in the random activation of synapses. This was achieved through tonic activation of all 1474 excitatory and all 105 GABAergic synapses. The tonic conductance of each synapse was equivalent in mean amplitude to that generated by its random activation. Through modulation of the peak conductance of the excitatory synapses we could, in addition, control the level of membrane depolarization. The stimulus consisted of a single IPSP elicited by a single synapse located in an apical compartment of branch b3s44 or branch b0s01 (see arrow in the PC model sketch in Fig. 2).

### Data analysis

We computed the average IPSP as the event-triggered average of the membrane potential. The trigger events were the input spikes randomly delivered to the selected synapse. The IPSP traces in Figs 2 and 3 plot the mean and SD of the event-triggered average. The baseline was the average membrane potential in the 200-ms prestimulus interval and the IPSP peak amplitude was defined as the maximum negative deviation from baseline within the 100 ms following the trigger event. The IPSP started at the trigger event and its rise time was the time needed for the potential to rise from 10 to 90% of the peak value. The same peak amplitude was used to calculate the full width at half-height of the IPSP. We defined the attenuation factor as the ratio of the peak amplitude in the postsynaptic compartment to that measured at the soma. Another metric, the

amplification factor, quantifies the effect of voltage-gated channels and was calculated as the ratio of the peak amplitude in the adPC to that in the pPC, measured either in the dendrite or at the soma. All data are given as mean  $\pm$  SD. Linear regression best fits were made using the MATLAB (The MathWorks, Natick, MA, USA) *robustfit* function. This algorithm uses iteratively reweighted least squares. New weights are computed based on the distance of each data point from the previous least-square fit. A point farther from the fit gets reduced weight. *P*-values indicate the result of Student's paired *t*-test comparison. The linear regression fit had a slope significantly different from 0 if  $P < 0.001$  unless otherwise stated. To quantify variability we used a non-parametric equivalent of the CV, the numerical CV (nCV). The nCV is the median absolute deviation from the median of the distribution divided by the median. This figure has the advantage of being less sensitive to outliers than the standard CV (i.e. the SD divided by the mean).

## Results

### *Inhibitory postsynaptic potentials generated by the activation of distal dendritic synapses*

#### *Compound inhibitory postsynaptic potentials*

We first examined the propagation of IPSPs along the PC dendrite and its dependency on the activation of voltage-gated ion channels. Two model PCs, a purely passive one (pPC) and one with an active dendrite (adPC), were driven by identical background spike trains with excitatory and inhibitory synaptic activation rates of 10 and 28 Hz, respectively (see Materials and methods). Tonic background activation of the voltage-gated ion channels depolarized at rest the soma and dendrite of the adPC by 15 mV with respect to the pPC (Jaeger *et al.*, 1997) (Fig. 2A and B). In order to monitor the propagation of IPSPs we superimposed on the background input an inhibitory stimulus which triggered the synchronous activation of 42 GABA<sub>A</sub> receptor synapses located on an apical PC model branch (see inset to Fig. 2). These GABA<sub>A</sub> receptor synapses did not mediate background input. We doubled the strength of the activated synapses to improve the signal-to-noise ratio, obtaining in this way a cIPSP having an amplitude at the soma three times larger than the peak-to-peak amplitude of the membrane potential noise (4.5 mV, data not shown). The synapses were activated at 0.5 Hz during 200 s. The cIPSP peak amplitude and the 10–90% rise time were measured at both the postsynaptic compartment and the soma. In both models we observed a significant reduction in amplitude and an increase in rise time between the cIPSPs recorded at the two sites (see Table 1).

In the passive model (pPC), dendritic low-pass filtering attenuated the peak amplitude by a factor of 12.7 at the soma and increased the rise time by a factor of almost 10 (see Table 1). Switching on the voltage-dependent ion channels in the dendrite (see adPC, Fig. 2B) partly compensated for the passive filtering, leading to an attenuation factor of only 7.1. Comparison of the cIPSPs elicited in the adPC and pPC showed that the activation of voltage-dependent ion channels caused a two-fold amplification of the peak amplitude of distally recorded cIPSPs. At the soma the amplification was even more pronounced yielding a multiplicative factor of 3.6.

The more depolarized resting membrane potentials of the adPC could have caused part of the amplification observed in the dendrite, as it doubled the inhibitory synaptic driving force. We therefore reduced the reversal potential of the GABAergic synapses located on the stimulated branch of the adPC from  $-80$  to  $-65$  mV, so as to produce currents and IPSPs of similar amplitudes in the stimulated compartments of the pPC and adPC (Fig. 2A and C and adPC\* in Table 1).

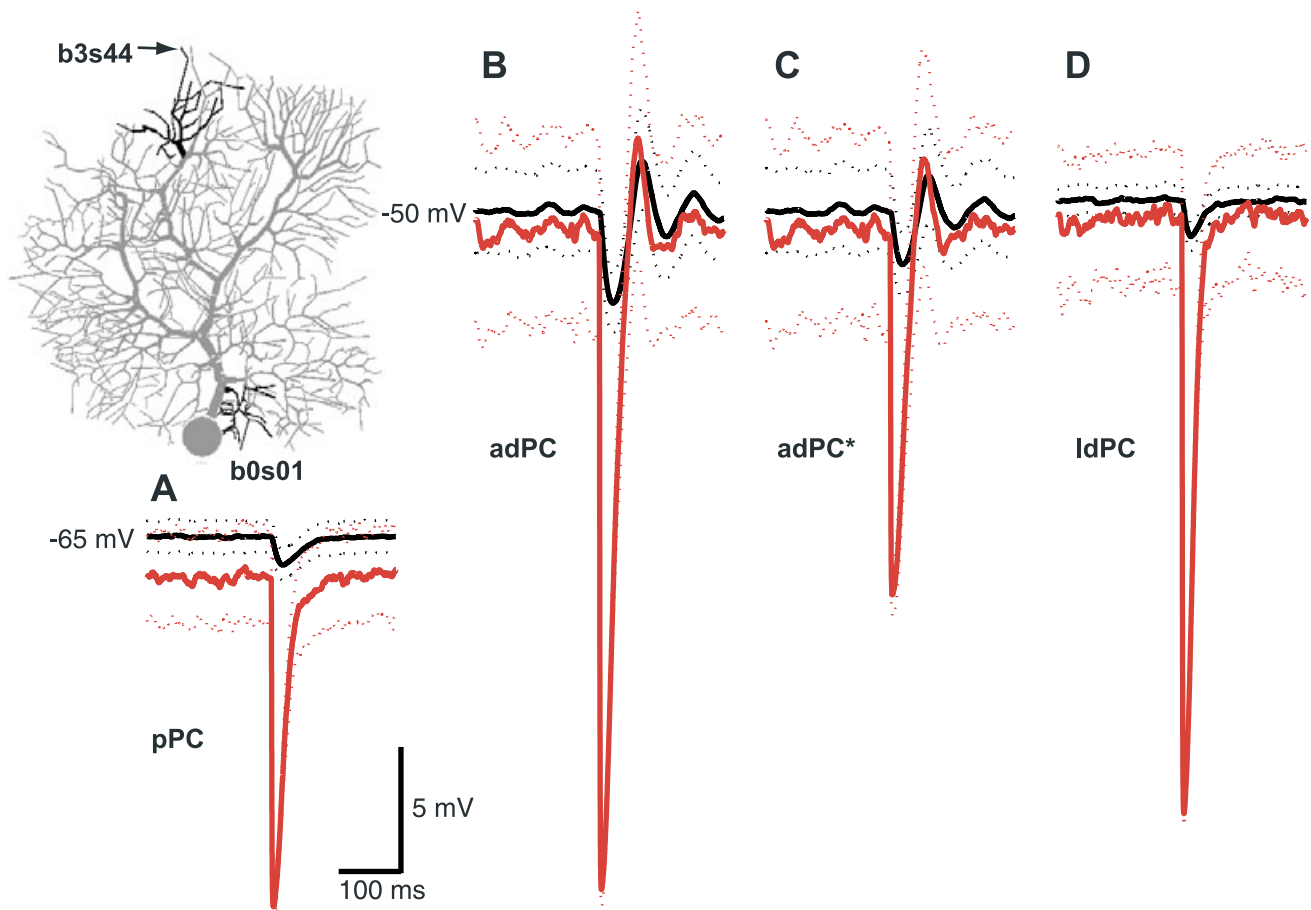


FIG. 2. The effect of passive and active membrane properties of the model Purkinje cell (PC) on the compound inhibitory postsynaptic potentials (IPSPs) elicited by the synchronous activation of 42 GABA<sub>A</sub> receptor synapses located on a distal branch. The inset reproduces the morphology of the model PC, with two dendritic branches marked in black: dendritic branches of the PC model b3s44 (apical) and b0s01 (perisomatic). The larger IPSPs observed in the postsynaptic compartment (gray traces) and soma (black) following stimulation of branch b3s44 in four versions of the model PC: the completely passive PC model (pPC, A); PC with an active dendrite but passive soma [active dendrite PC model (adPC), B]; adPC after the reversal potential of the GABAergic currents was changed from  $-80$  to  $-65$  mV in order to obtain the same synaptic driving force at rest (15 mV) as in the pPC (adPC\*, C) and pPC with the passive membrane properties of each compartment adjusted so as to obtain the same leakage current as in the corresponding compartment of the adPC [leaky-dendrite passive PC model (ldPC), D]. The compound inhibitory postsynaptic potentials were calculated by event-triggered-average analysis (see Materials and methods). The dotted lines show the SD obtained from 100 stimulus repetitions.

This reduction in synaptic driving force in the adPC reduced the peak amplitude of the somatic cIPSPs to 58% of the normal value (see Table 1) but the cIPSPs in this modified adPC were still larger by a factor of 2.1 than those produced in the pPC ( $P < 0.0001$ ).

Apart from generating a more depolarized resting membrane potential, active channels reduce the overall membrane resistance, resulting in both a longer compartmental electrotonic length and a smaller membrane time constant (Rall & Among-Snir, 1998). As fast membrane potential transients are better preserved by compartments with a small time constant but decay more rapidly when traveling along compartments with a long electrotonic length, the effect of an increase in membrane conductance cannot be easily predicted (Kuhn *et al.*, 2004). We therefore modified the pPC so that the membrane resistance and resting potential of each compartment matched their effective values in the adPC driven by background input, and obtained a pPC version with a leakier dendrite. In this configuration, the pPC had the same passive properties and resting potentials as the adPC (compare Fig. 2B and D). The dendritic IPSP peak amplitude and time-course were also similar in the adPC and leaky-dendrite passive PC model. Nevertheless, the somatic IPSP

was much smaller in the leaky-dendrite passive PC model than the adPC and did not show the rebound oscillations characteristic of the voltage-dependent ion channel dynamics (Fig. 2B and D). Hence, changes in the synaptic driving force or membrane resistance cannot explain the apparent amplification of somatic IPSPs by an active dendrite.

#### Unitary inhibitory postsynaptic potentials

Voltage-gated ion channels are non-linearly dependent on the membrane potential and thus the cIPSP, more than 80 times larger than a unitary IPSP, could have been amplified by an unphysiological change in activation of voltage-gated inward currents. Likewise, saturation of the IPSPs in the postsynaptic compartments could have led to an underestimation of the degree of attenuation at the soma. We therefore also measured the unitary IPSPs mediated by single synapses receiving the background input only. The reversal potential of all GABAergic synapses was set to the original value of  $-80$  mV. The pPC and adPC were simulated for 400 s, each inhibitory synapse being activated an average of 11 000 times. The membrane potentials of all compartments that received a stellate-cell synapse, 105 in total

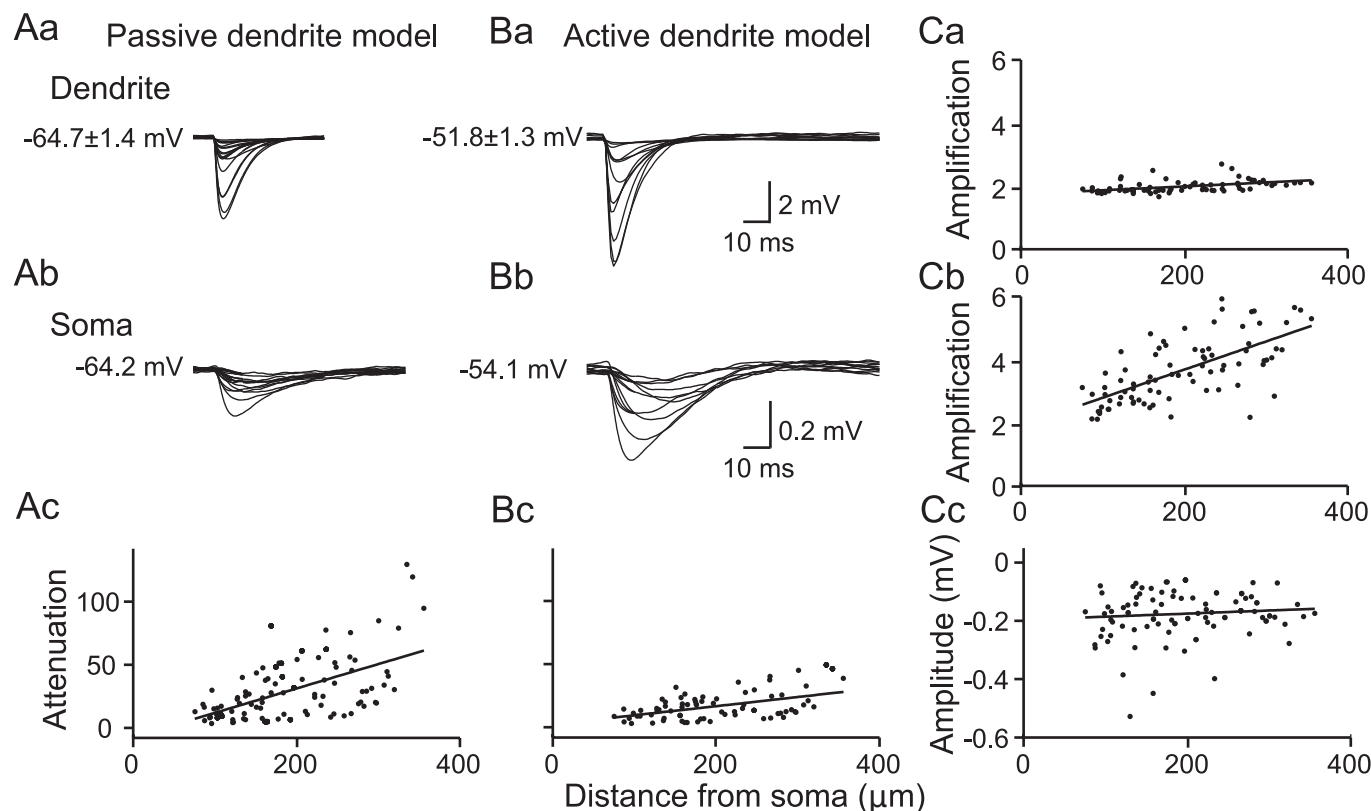


FIG. 3. Unitary inhibitory postsynaptic potentials (IPSPs) elicited by the activation of individual synapses at various locations along the dendritic tree. (A) Superimposed sample averaged IPSPs measured in the postsynaptic compartment (Aa) and soma (Ab) of the completely passive Purkinje cell model (pPC). Each trace is the event-triggered average of the membrane potential for 11 000 incoming spikes used as trigger events. The mean  $\pm$  SD of the baseline is indicated on the left. The SD of the somatic traces was less than 0.003 mV. Ac plots, for each of the 105 activated synapses, the amount of attenuation of the somatic IPSP relative to the IPSP in the postsynaptic compartment (see Materials and methods) as a function of the distance of the synapse from the soma. (B) Same format as A, for IPSPs recorded in the active dendrite Purkinje cell model (adPC). The weighted linear regression fits showed a significant positive correlation in both models ( $P < 0.0001$ ). (C) The active adPC and passive pPC compared. (Ca) The amplification factors (see Materials and methods) for the IPSPs in the postsynaptic compartments as a function of synaptic distance from the soma. (Cb) Amplification of the somatic IPSPs. (Cc) Peak amplitude of somatic IPSPs recorded in the adPC.

TABLE 1. Compound inhibitory postsynaptic potential (cIPSP) transformation

Model	Peak amplitude (mV)		Rise time (ms)	
	Dendrite	Soma	Dendrite	Soma
pPC	12.7 $\pm$ 0.4	1.0 $\pm$ 0.6	1.32 $\pm$ 0.06	11.2 $\pm$ 0.9
adPC	25.6 $\pm$ 0.6	3.6 $\pm$ 1.2	0.9 $\pm$ 0.2	12.2 $\pm$ 0.4
adPC*	14.2 $\pm$ 0.8	2.1 $\pm$ 1.2	0.9 $\pm$ 0.2	10.9 $\pm$ 0.5
ldPC	25.5 $\pm$ 0.6	1.5 $\pm$ 0.6	1.0 $\pm$ 0.2	8.6 $\pm$ 0.5

The cIPSP peak amplitude and 10–90% rise time (mean  $\pm$  SD) measured at the soma and the postsynaptic compartment in different versions of the Purkinje cell (PC) model (see Materials and methods). In the adPC\*, the reversal potential of the synapses mediating the compound stimulation was changed to  $-65$  mV. The leaky-dendrite passive PC model (ldPC) is completely passive but the reversal potential and conductance of the leak current of each compartment were set to the effective values measured in the corresponding compartment of the active dendrite PC model (adPC). pPC, completely passive PC model.

(see Materials and methods), were recorded, as well as the currents through their voltage-gated ion channels and the somatic membrane potential.

In both the pPC (Fig. 3A) and adPC (Fig. 3B) the unitary IPSPs measured at the soma were an order of magnitude smaller than those generated in the postsynaptic compartments (note the large difference

in vertical scale for the somatic and dendritic IPSPs). The attenuation of the IPSP peak amplitude from the postsynaptic compartment to the soma was larger, and more strongly correlated to synaptic distance, in the pPC (Fig. 3, Ac, slope best fit  $0.1932 \mu\text{m}^{-1}$ , range  $0.1358$ – $0.2507 \mu\text{m}^{-1}$ ,  $R^2 = 0.3$ ) than the adPC (Fig. 3, Bc, slope best fit  $0.0726 \mu\text{m}^{-1}$ , range  $0.0449$ – $0.1003 \mu\text{m}^{-1}$ ,  $R^2 = 0.22$ ). The effect of the active membrane on IPSP propagation is illustrated more explicitly in Fig. 3, Ca and Cb, which plots the amplification of the IPSP amplitude in the adPC relative to the pPC (amplification factor, see Materials and methods) as a function of dendro-somatic path length (Fig. 3, Ca, dendritic IPSPs, slope best fit  $0.0012 \mu\text{m}^{-1}$ , range  $0.0008$ – $0.0016 \mu\text{m}^{-1}$ ,  $R^2 = 0.25$ ; Fig. 3, Cb, somatic IPSPs, slope best fit  $0.0089 \mu\text{m}^{-1}$ , range  $0.0068$ – $0.0110 \mu\text{m}^{-1}$ ,  $R^2 = 0.43$ ). The amplification factor calculated at the postsynaptic compartment had a slight but significant ( $P < 0.00001$ ) dependency on the synaptic distance from the soma. As for the cIPSPs the mean amplification factor was equal to 2. When measured at the soma, however, the amplification was much higher and varied from 2 to 6 from proximal to distal synapses, respectively ( $P < 0.00001$ ). Thus, the active membrane most strongly amplified the IPSPs elicited at distal synapses. As a result, the amplitudes of the somatic IPSPs were independent of the synaptic location in the adPC (Fig. 3, Cc, slope best fit  $0.000106 \text{ mV}/\mu\text{m}$ ,  $P = 0.7$ ,  $R^2 = 0.001$ ) as opposed to the pPC (not shown, slope best fit,  $-0.00014 \text{ mV}/\mu\text{m}$ ). Nevertheless, the amplitudes of the somatic IPSPs in the adPC were still variable (nCV

0.37). Part of this variability was generated by the scaling of each synaptic peak conductance to the surface area of its postsynaptic compartment (nCV 0.68, see Materials and methods). The nCV of the IPSP amplitudes measured at the site of generation was 0.82. In the pPC we measured an nCV of 0.48 and 0.77 for the somatic and dendritic IPSP amplitudes, respectively. The remaining variability should be attributed to the dendritic architecture as the membrane potential was approximately constant over all the model compartments (Fig. 3, Aa and Ba). Thus, the presence of the voltage-gated ion channels enhanced the variability of the IPSP amplitudes in the dendrite and reduced it at the soma (De Schutter, 1998).

All IPSPs had a similar time-course at their site of origin (Fig. 4A and B). In both model versions the IPSP rise time and width measured at the postsynaptic compartment were not correlated to the synaptic distance from the soma (Fig. 4A and B upper panels; pPC, rise time  $3.1 \pm 0.6$  ms,  $R^2 = 0.0036$ , width  $9.3 \pm 2.1$  ms,  $R^2 = 0.0015$ ; adPC, rise time  $3.4 \pm 1.0$  ms,  $R^2 = 0.0002$ , width  $10.8 \pm 3.5$  ms,  $R^2 = 0.0052$ ;  $P$ -value of the best fit slopes  $>0.1$ ). At the soma, in contrast, IPSPs elicited at more distal synapses in the pPC had a longer rise time (Fig. 4A lower left panel; best fit slope  $0.0379 \mu\text{m}^{-1}$ , range 4.1–27.0 ms,  $R^2 = 0.25$ ) and width (Fig. 4A lower right panel; best fit slope  $0.0476 \mu\text{m}^{-1}$ , range 12.8–51.1 ms,  $R^2 = 0.18$ ) as predicted by passive cable theory. In the adPC, the somatic IPSP rise time was also linearly dependent on the distance of the synapse from the soma (Fig. 4B lower left panel; best fit slope  $0.0317 \mu\text{m}^{-1}$ , range 5.3–21.6 ms,  $R^2 = 0.45$ ) and the difference from the pPC was small and statistically not significant ( $P > 0.1$ ). Thus, the rise time of somatic IPSPs was not affected by the voltage-gated ion channels. Conversely, the dependency of the width on the synaptic distance from the soma showed a significant difference between the adPC and pPC versions. The width of somatic IPSPs in the adPC did not depend on the synaptic location (Fig. 4B lower right panel; best fit slope  $0.0076 \mu\text{m}^{-1}$ ,  $P > 0.05$ , mean  $23.0 \pm 3.2$  ms, range 10.3–30.2 ms,  $R^2 = 0.027$ ).

#### Mechanism of inhibitory postsynaptic potential amplification

As shown above, voltage-dependent ion channels increased the peak amplitude and shortened the decay phase of the somatic IPSPs evoked by the activation of distal synapses. The IPSP rise time was unaffected. We next examined the contribution to the IPSP amplification made by  $\text{Ca}^{2+}$  and  $I_h$  currents, which have been reported to modify the propagation of postsynaptic potentials (see Discussion). To this end, we simulated the adPC with the  $\text{Ca}^{2+}$  or  $I_h$  currents partly or completely blocked. Figure 5 shows that completely blocking the  $I_h$  current did not affect the IPSP amplification. In contrast, decreasing the density of  $\text{Ca}^{2+}$  channels had two effects. First, the fall in inward current uniformly hyperpolarized the entire neuron and the resulting reduction of the synaptic driving force decreased the IPSP amplitude for all synaptic locations by the same factor. This led to a downward displacement of the linear-regression lines on the amplification diagram (Fig. 5, dendritic IPSPs, dashed lines). The second, more important effect was a drastic reduction of the slope of the amplification curve of the somatic IPSPs when the density of  $\text{Ca}^{2+}$  channels was reduced from 70 to 60% (Fig. 5, somatic IPSPs, solid lines). The somatic best-fit regression slope now approached the dendritic amplification factors, which implies a selective loss of amplification of the IPSPs evoked by distal synapses. Thus, the amplification of distally evoked IPSPs was strongly dependent on the presence of  $\text{Ca}^{2+}$  channels in the dendrite.

In order to understand the dynamics of the amplification mechanism, we examined in greater detail the activation of ionic channels in the postsynaptic and somatic compartments of the adPC with the

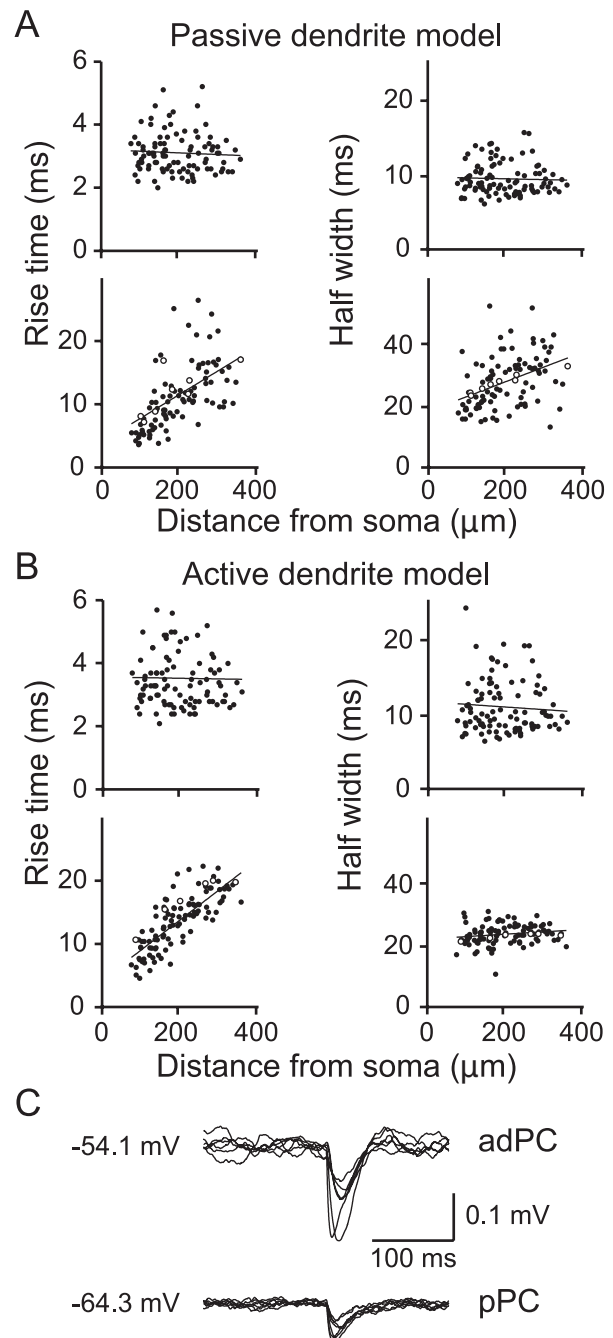


FIG. 4. The effect of passive and active membrane properties on the time-course of unitary inhibitory postsynaptic potentials (IPSPs). 10–90% rise time and full-width-at-half-height of IPSPs measured in the postsynaptic compartment (upper panels) and soma (lower panels) of the completely passive Purkinje cell model (pPC) (A) and active dendrite Purkinje cell model (adPC) (B). Each panel shows data for 105 locations of stellate-cell synapses. (C) Representative examples of IPSPs recorded at the soma in the adPC (top) and pPC (bottom). Their rise times and widths are plotted as open symbols in the lower panels of A and B.

original density of  $\text{Ca}^{2+}$  channels. We removed the noise inherent in the random activation of synapses by clamping each synapse's conductance, except for the stimulated one, to the mean conductance generated originally (i.e. by the combined excitatory and inhibitory activation rates of 10 and 28 spikes/s). In this configuration the tonic activation of ion channels yielded a stable membrane potential of  $-50$  mV (Fig. 6B, middle column), similar to that of the adPC when

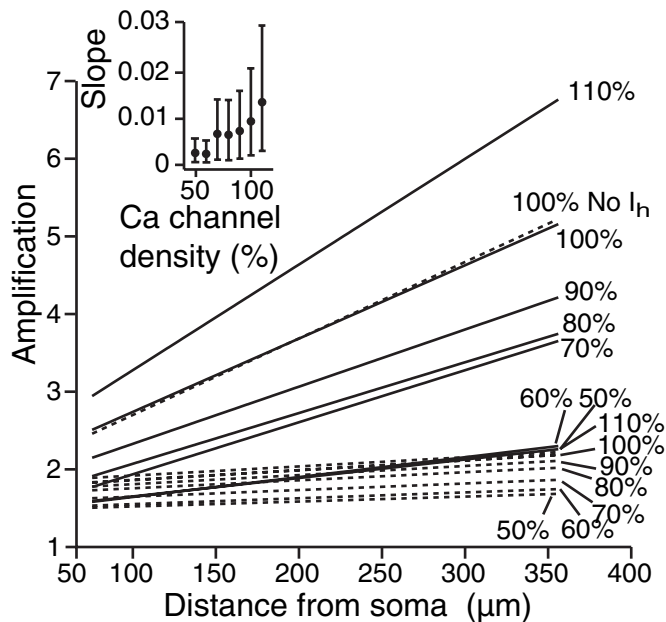


FIG. 5. The amplification of unitary inhibitory postsynaptic potentials (IPSPs) depends on the density of high threshold activated  $\text{Ca}^{2+}$  current (P-type  $\text{Ca}^{2+}$ ) channels but not on the hyperpolarization-activated mixed cationic current ( $I_h$ ). Each curve is the linear regression line of the relationship between the degree of IPSP amplification and the distance of the activated synapse from the soma (as illustrated in Fig. 3, Ca and Cb). The amplification factors were measured at the postsynaptic compartments (dashed lines) or soma (solid lines). The density of P-type channels was varied from 50 up to 110% of its original value ( $4.5 \text{ mS/cm}^2$ ) in the active dendrite Purkinje cell model. A separate simulation was run with the  $I_h$  current completely blocked and the original density of P-type channels (upper dashed line). The inset shows the slopes of the linear regression fits of the amplification factors at the soma plotted for the varying densities of P-type  $\text{Ca}^{2+}$  channels.

driven by a noisy background input (Fig. 2B). We recorded the  $\text{Ca}^{2+}$  and  $\text{K}^+$  currents and the membrane potential in one compartment of an apical branch (see arrow in the inset of Fig. 2). A unitary IPSP was generated in the compartment itself. In both the apical and perisomatic branches, the most apparent changes were a decrease in magnitude of the P-type  $\text{Ca}^{2+}$  current and a delayed decrease of the  $\text{Ca}^{2+}$ -activated  $\text{K}^+$  currents (Fig. 6A, middle traces). The activation variable of the P-type  $\text{Ca}^{2+}$  channel faithfully followed the IPSP time-course, reaching 60% of its steady-state value at the IPSP peak (data not shown). The inactivation variable, in contrast, was unaffected by the IPSP because of its slow dynamics (De Schutter & Bower, 1994a). The time-courses of the two  $\text{Ca}^{2+}$ -activated  $\text{K}^+$  currents, KC and K2 in Fig. 6A, were almost identical, reaching their peak decrease after the  $\text{Ca}^{2+}$  current. The activation of the  $\text{Ca}^{2+}$ -activated  $\text{K}^+$  currents was controlled by the product of a voltage- and a  $\text{Ca}^{2+}$ -dependent factor (De Schutter & Bower, 1994a). While the voltage-dependent factor followed the IPSP time-course, and reached 76% of its steady-state value, the  $\text{Ca}^{2+}$ -dependent factor followed the integral of the  $\text{Ca}^{2+}$  current (data not shown). In the present model, the delayed rectifier and the A-type potassium channel were restricted to the main dendrite and did not affect IPSP amplification. Likewise, the changes induced in the T-type  $\text{Ca}^{2+}$  current and persistent  $\text{K}^+$  currents were too slow and small (less than 20 and 18%, respectively) to amplify the IPSP (see Fig. 6A).

With regard to the  $I_h$  current, the maximum change that we observed in the distal branch was 17% of the steady-state current. In order to enhance the contribution of the  $I_h$  current, whose channel had

a  $V_{1/2}$  of  $-73.2 \text{ mV}$  (see Materials and methods), we next hyperpolarized the PC to  $-70 \text{ mV}$  by reducing the excitatory load to 60% of control and adjusted the equilibrium potential of the stimulated inhibitory synapses so as to keep their driving force equal to  $30 \text{ mV}$ . In this configuration, the  $\text{Ca}^{2+}$  current was strongly reduced and the  $\text{Ca}^{2+}$ -activated  $\text{K}^+$  channel closed almost completely (Fig. 6A, left traces). Conversely, the amplitude of the  $I_h$  current increased to  $3.3 \text{ mA/m}^2$ . The IPSPs recorded at the postsynaptic compartment and soma were similar in amplitude to the controls (Fig. 6B). The somatic IPSPs were larger by a factor of 4 than those produced in the pPC (dashed traces in Fig. 6B) and this amplification was only partially due to the reduced driving force of the pPC. Hence, in this hyperpolarized configuration, the IPSP was amplified by a deactivation of the  $\text{Ca}^{2+}$  current which was not counteracted by deactivation of the  $\text{K}^+$  current, leading to preservation of the IPSP amplification and enhancement of the IPSP tail. Incorporating the  $I_h$  current in the pPC reduced the IPSP amplitude by 4% (Fig. 6B, lower left panel) and accelerated the decay, consistent with previous results (Roth & Häusser, 2001; Williams & Stuart, 2003b).

Thus, over a broad range of resting potentials, the inward  $\text{Ca}^{2+}$  current was strongly deactivated by the IPSPs, causing the IPSP amplification. Delayed deactivation of the  $\text{Ca}^{2+}$ -activated  $\text{K}^+$  channel depolarized the membrane, shortcircuiting the IPSP and reactivating the  $\text{Ca}^{2+}$  and  $\text{K}^+$  currents. This mechanism was iterated a couple of times generating the observed small oscillations of somatic IPSPs (see Fig. 2B), which are more pronounced at more depolarized potentials (Fig. 6B, right traces). Finally, while deactivation of the  $\text{Ca}^{2+}$  current was responsible for IPSP amplification, deactivation of the  $\text{K}^+$  current limited IPSP amplification and shortened the IPSP decay. This effect was not observed for hyperpolarized membrane potentials (Fig. 6B, left traces).

This fact, together with the observation that distally elicited IPSPs were more amplified than proximal ones, suggested that distal inhibitory synapses would also deactivate  $\text{Ca}^{2+}$  channels in neighboring compartments, in a manner similar but opposite in sign to the amplification mechanism described for EPSPs (De Schutter & Bower, 1994b). We therefore recorded the current through the P-type  $\text{Ca}^{2+}$  current channel of each dendritic compartment, following the activation of a single synapse. Figure 7A shows, for two locations of the activated synapse, the decrease in amplitude of the  $\text{Ca}^{2+}$  currents, plotted as a function of the distance of each compartment from the activated synapse.

The data points corresponding to compartments of the same dendritic branchlet formed clusters. When the stimulated compartment was perisomatic (e.g. branch b0s01), only a few nearby compartments showed large changes in current amplitude (the small cluster in the upper left-hand corner of Fig. 7A). Moving the stimulation site to the apical branch b3s44, the compartments belonging to this branch individually showed a smaller  $\text{Ca}^{2+}$  current change but the number of compartments where  $\text{Ca}^{2+}$  current changed more than  $10^{-4} \text{ A/m}^2$  was much larger, yielding more data points in the highest cluster (right panel of Fig. 7A). Thus, IPSPs elicited in more distal branches were able to deactivate a larger number of  $\text{Ca}^{2+}$  channels. Hence, while at the postsynaptic site itself the changes in  $\text{Ca}^{2+}$  current can be bigger for proximal than for distal synaptic inputs, the overall transmembrane  $\text{Ca}^{2+}$  current (summed along the entire dendritic tree) decreased more strongly when the activated synapse was more distally located (Fig. 7B).

#### Effects of inhibition on the Purkinje cell firing pattern

The attenuation of the IPSPs elicited by many distal synapses of the pPC and adPC indicated that most of their hyperpolarizing effects

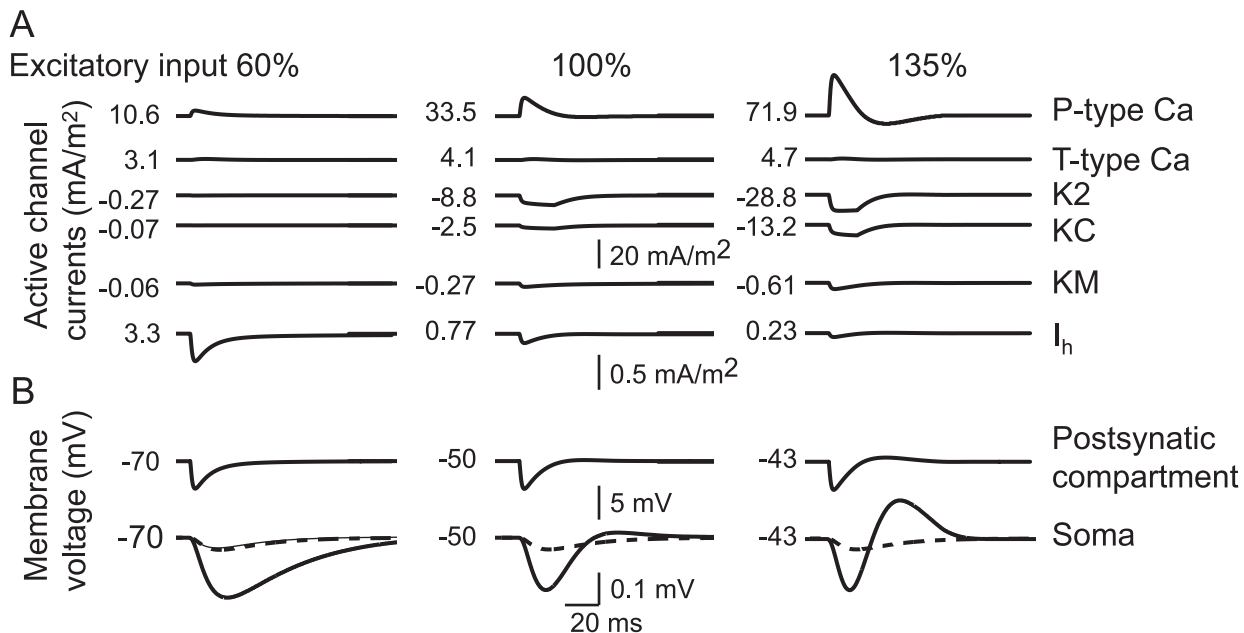


FIG. 6. The Ca<sup>2+</sup> currents and Ca<sup>2+</sup>-gated K<sup>+</sup> currents are responsible for the non-linear transformation of the unitary inhibitory postsynaptic potentials (IPSPs). Three simulations of the active dendrite Purkinje cell model (adPC) are illustrated, characterized by a steady-state conductance of the excitatory synapses set equal to 60, 100 and 135% of the default value (see Materials and methods) from left to right, respectively. The IPSP mediated by a single synapse was triggered at the apical compartment of branch 44. For each trace, the steady-state value is shown on the left and inward positive currents are drawn downward. (A) Time-course of the P-type current, the K2 and KC Ca<sup>2+</sup>-dependent K<sup>+</sup> currents, the muscarinic-sensitive K current and the hyperpolarization-activated mixed cationic current (I<sub>h</sub>), measured in the postsynaptic compartment. (B) Time-course of the membrane potentials in the postsynaptic and somatic compartments [dashed lines show corresponding IPSPs in the completely passive Purkinje cell model (pPC)]. The lower left panel plots in addition the somatic IPSP generated in the pPC into which the I<sub>h</sub> current of the adPC was incorporated (thin solid line).

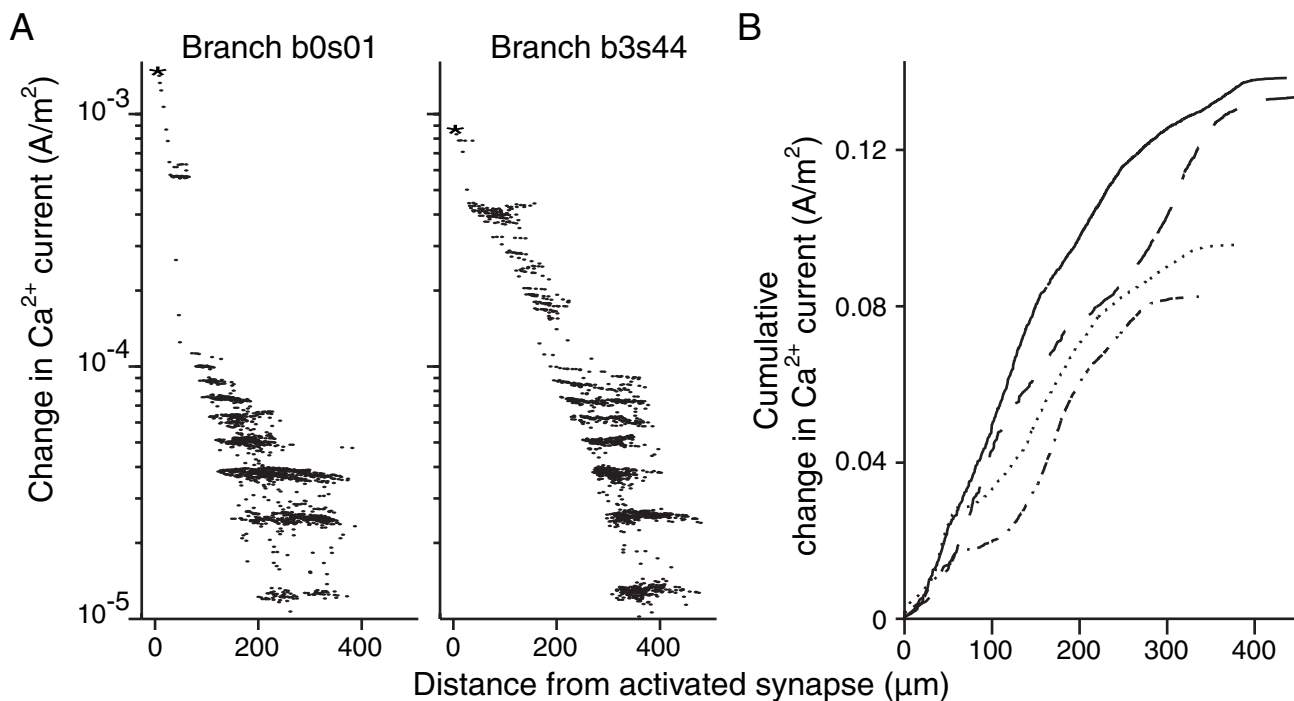


FIG. 7. (A) The decrease in Ca<sup>2+</sup> current from steady-state flux, measured in each Purkinje cell (PC) compartment, triggered by eliciting a unitary inhibitory postsynaptic potential (IPSP) in a perisomatic (dendritic branch of the PC model b0s01, left) or apical (dendritic branch of the PC model b3s44, right) branch. Each of the 1700 data points represents the decrease in peak amplitude of the P-type Ca<sup>2+</sup> current of one compartment, whose distance from the activated synapse is plotted on the horizontal axis. The largest decrease in Ca<sup>2+</sup> current was recorded in the compartment in which the IPSP was elicited (\* in the plot). The currents were normalized by each compartment's surface area. (B) Cumulative plots of the change in Ca<sup>2+</sup> current triggered in the postsynaptic compartment and in the compartments located within the distance shown on the horizontal axis. Distance was measured along the dendritic path. The four lines show data recorded after stimulation of synapses located on branches b0s01 (evenly dotted line), b2s21 (lowest curve, unevenly broken line), b1s18 (top, unbroken line) and b3s44 (evenly dashed line). The four synapses were separated from the soma by 86, 168, 239 and 305 μm along the dendritic path, respectively.

were restricted to the dendrite. Thus, apical and perisomatic inhibitory synapses might control different features of the PC firing pattern. We investigated the effect of the dendritic and somatic inhibitory input in shaping the firing pattern of the aPC. In previous studies using the original PC model (De Schutter & Bower, 1994a), inhibition at the dendrite was found to be determinant in achieving a physiological output firing pattern (De Schutter & Bower, 1994b; Jaeger *et al.*, 1997; Jaeger & Bower, 1999), i.e. a CV close to 1. Here we investigate the effect of perisomatic inhibition on the firing pattern of the aPC. We simulated the aPC and systematically varied the distribution of the peak conductances and activation rates over the dendritic (stellate cell) and perisomatic (basket cell) synapses. The AMPA receptor synapses were activated at 10 spikes/s in all simulations. Each individual stellate-cell input to the dendritic branches was distributed over nine synapses (see Materials and methods).

In the first simulation set (left panels in Fig. 8) the peak conductances of the GABA<sub>A</sub> receptor synapses were left unchanged

(see Materials and methods) but the random activation frequency of the stellate cell synapses was decreased run after run from 40 to 20 spikes/s, while that of basket-cell synapses was increased from 0 up to 31 spikes/s. These balanced modifications kept the aPC firing at a constant rate of  $38.1 \pm 0.3$  spikes/s. The irregularity of the aPC firing pattern was not affected by a shift from a pure dendritic to a partially somatic inhibitory input ( $P > 0.2$ ) so long as this was induced by changes of the activation rates of the synapses. In a second simulation set (right panels in Fig. 8), the peak conductances of dendritic inhibitory synapses were decreased (from 100 to 59% of its regular value) while those of somatic synapses were raised (from 0 to 1000% of its regular value). Although the change in balance between total synaptic current between dendrites and soma was similar (upper panels of Fig. 8), increasing the amplitude of somatic IPSCs significantly increased the variability of the aPC firing pattern (regression best fit slope  $0.0094 \pm 0.0010$ , CV range 0.75–1.22,  $P < 0.00001$ ).

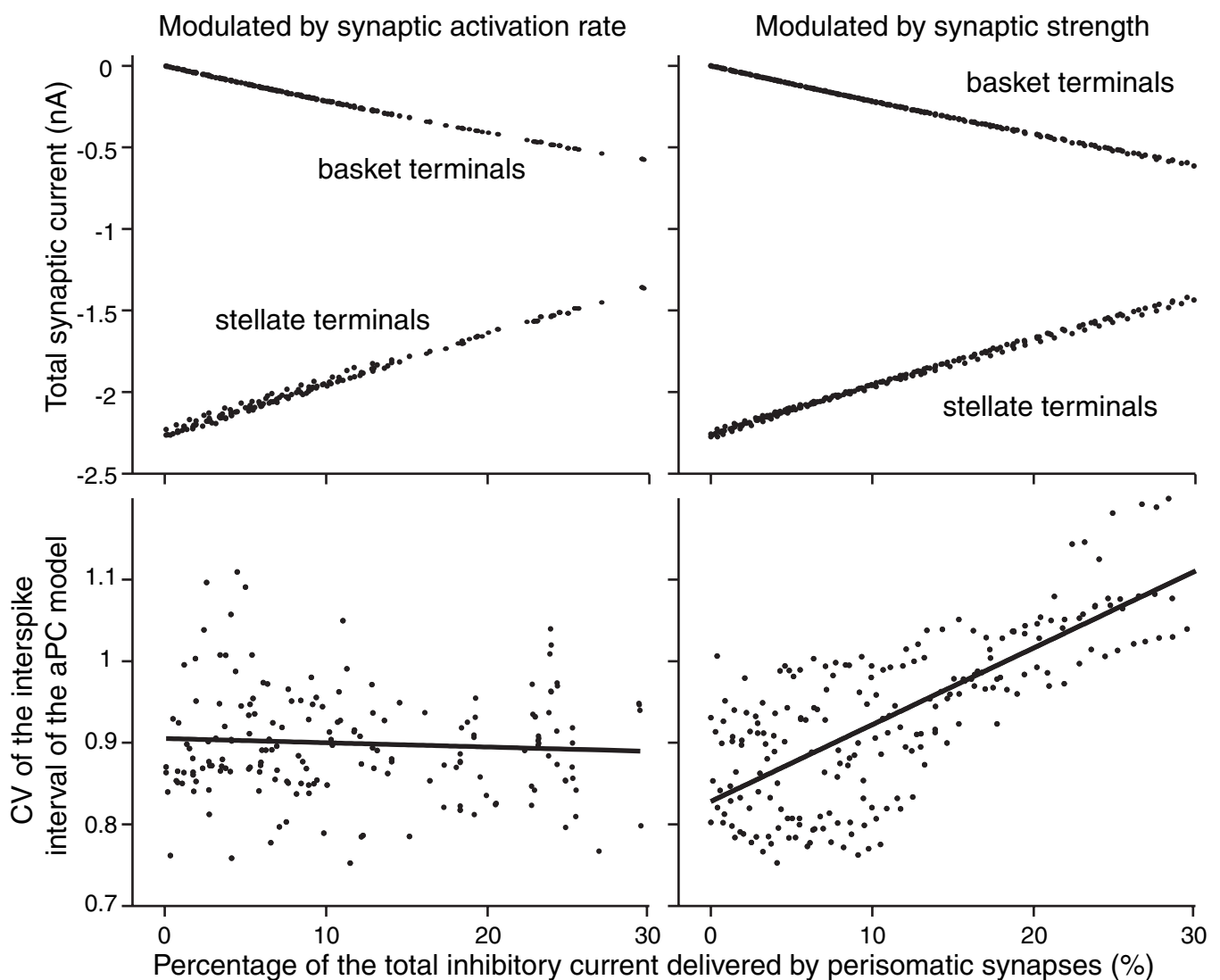


FIG. 8. The efficacy of perisomatic vs. dendritic inhibitory input in the control of the irregularity of the Purkinje cell firing pattern. The upper panels show the total currents mediated by GABAergic synapses located on the apical dendrites (stellate cell synapses) and on the main dendrite and soma (basket cell synapses). Each pair of points represents one simulation of 3–5-s duration of the completely active Purkinje cell model (aPC). The lower panels plot the resulting coefficient of variation (CV) of the interspike interval of the aPC. The horizontal axes measure the relative share of current mediated by basket cell synapses. In the left panels, the balance between stellate and basket cell input was modulated by varying the corresponding synaptic activation rates; in the right panels, the synaptic peak conductances were varied.

## Discussion

Cable theory predicts that postsynaptic potentials undergo a significant attenuation and broadening when they propagate in large neurons from distal dendrites to the soma (Rall, 1970; Rall & Among-Snir, 1998). Cable theory applies, however, to passive membranes and the effects of voltage-gated ion channels on the postsynaptic potentials cannot be easily predicted. The interaction of dendritic ion channels with synaptic signals is of particular interest in cerebellar PCs as these neurons have an extremely large number of synaptic contacts (Harvey & Napper, 1991) located on very active dendrites with a high density of  $\text{Ca}^{2+}$  channels (Eilers *et al.*, 1996). We have previously used a detailed PC model to predict that activation of excitatory parallel-fibre synapses will open dendritic  $\text{Ca}^{2+}$  channels and that this effect is more pronounced in the distal dendrite. This leads to a differential amplification of somatic EPSPs which can largely compensate for the passive attenuation (De Schutter & Bower, 1994c). These model predictions have been partially confirmed experimentally (Eilers *et al.*, 1996) and differences between simulation and experiment may be explained by differences in holding potentials (De Schutter & Steuber, 2000). Here we extend this study to the effect of dendritic voltage-gated channels on IPSPs.

Using an updated version of the same PC model we found that IPSPs, like EPSPs, were amplified by the dendritic  $\text{Ca}^{2+}$  channels. Thanks to advances in computing power we could study this amplification in more detail for IPSPs. In particular, we simulated the attenuation of both compound (Fig. 2) and unitary (Fig. 3) IPSPs while only compound EPSPs were investigated previously. We first elicited cIPSPs to take advantage of the higher signal-to-noise ratio for data analysis. Using the cIPSPs we could estimate that changes in synaptic driving force can contribute up to a factor of 2 to the amplification. Moreover, we could demonstrate the lack of involvement of other passive mechanisms in the IPSP transformation. We did not observe fundamental differences between amplification of cIPSPs and unitary IPSPs. For unitary somatic IPSPs we found the amplification factor, which ranged from 2 to 6, to be insufficient to fully compensate for the dendritic attenuation (Fig. 3, Bc). A relevant difference with the amplification of (compound) EPSPs is that the width of the somatic IPSP was independent of the distance of the synaptic contact from the soma (Fig. 4B) while the rise time still increased with distance.

### Mechanisms

Changes in driving force have more effect on inhibitory synaptic currents than on excitatory ones because the inhibitory reversal potential is much closer to the membrane potential. As dendritic  $\text{Ca}^{2+}$  channels depolarized the dendrite, the driving force for inhibitory synapses was increased, leading to larger IPSPs but this could only partially explain the difference with the passive dendrite (Fig. 2C). Similarly, the differences could not be explained by the change in membrane conductance caused by the dendritic voltage-gated channels (Fig. 2D).

We investigated the mechanisms responsible for the amplification in more detail. As for the amplification of EPSPs (De Schutter & Bower, 1994c), we could demonstrate a direct effect of the dendritic  $\text{Ca}^{2+}$  channels on IPSP amplification by changing the channel densities (Fig. 5). Calcium channels can amplify IPSPs if they are tonically active, as is presumably the case in an *in vivo* spontaneously firing PC, here simulated by driving the cell with background synaptic input (De Schutter & Bower, 1994b; Jaeger *et al.*, 1997; Jaeger & Bower, 1999). The hyperpolarization caused by the IPSP deactivated the  $\text{Ca}^{2+}$

channel (Fig. 6), leading to less positive current inflow and a further increase of the hyperpolarization. The decreased  $\text{Ca}^{2+}$  influx also led to a deactivation of the dendritic  $\text{Ca}^{2+}$ -activated  $\text{K}^+$  channels. This could have counteracted the amplifying effect but, because the  $\text{K}^+$  channel deactivation occurred later than the  $\text{Ca}^{2+}$  channel deactivation (Fig. 6A), it effectively cut off the amplification after a delay and explained the constant width of the amplified IPSPs. The  $\text{Ca}^{2+}$  channel deactivation was strongly voltage-dependent, being enhanced at increasing depolarization and reduced at lower membrane potentials (Fig. 6A). The deactivation of  $\text{Ca}^{2+}$ -activated  $\text{K}^+$  channels did not occur at hyperpolarized levels resulting in an increased width of the amplified IPSP (left panels of Fig. 6).

The cause of the larger amplification of distally compared with proximally evoked somatic IPSPs was the same as for the differential amplification of EPSPs (De Schutter & Bower, 1994c), i.e. a difference in local input impedances in the dendrite. The distal PC dendrite comprises mostly small spiny branches with little input impedance mismatches at branching points. This favors an extensive local spread of hyperpolarization to neighboring branches in the distal dendrite. In the proximal dendrite, spiny branchlets are connected to the thick smooth dendrite. Once the hyperpolarizing charge enters the smooth dendrite the impedance mismatch at the origin of other spiny branchlets is so large that the hyperpolarization cannot invade other spiny branchlets, leading to a much smaller local spread. Therefore, activation of proximal synapses will cause a pronounced  $\text{Ca}^{2+}$  channel deactivation only in a few compartments of the model while the more extensive spread following activation of a distal synapse causes deactivation in many compartments (Fig. 7). This mechanism is driven by the morphology of the PC dendrite and was shown to apply also to other PC models (Roth & Häusser, 2001), where the passive membrane properties are different from our model.

### Comparison to pyramidal neurons

The dendro-somatic transformation of IPSPs has been studied in pyramidal neurons in CA3 hippocampus (Miles *et al.*, 1996; Szilagyi & De Schutter, 2004) and neocortex (Stuart *et al.*, 1999; Williams & Stuart, 2003b). In neocortical layer 5 pyramidal neurons, Williams & Stuart (2003b) found that the persistent  $\text{Na}^+$  current and the mixed cationic  $I_h$  current significantly reshape the IPSPs depending on the level of dendritic depolarization. Contrary to our results they found the somatic IPSP width to be constant at hyperpolarized potentials only. These differences can easily be explained by the different voltage-gated channels involved. Deactivation of the persistent  $\text{Na}^+$  current leads to IPSP amplification but there is no secondary effect of the reduced  $\text{Na}^+$  influx as is the case for  $\text{Ca}^{2+}$  which, in the PC model, led to a constant half-width at depolarized potentials. The effect on IPSP width in pyramidal neurons is due to  $I_h$  which is activated only at hyperpolarized levels. In pyramidal neurons the  $I_h$  channel density can vary from 30 to 3  $\text{mS}/\text{cm}^2$  (Berger *et al.*, 2001) along the dendrite, whereas detailed model PCs having a uniform density 1000 times smaller, 25  $\mu\text{S}/\text{cm}^2$ , reproduced the time-dependent rectification observed in experiments (Roth & Häusser, 2001). Considering the large difference in  $I_h$  densities it is not surprising that dendritic  $I_h$  channels (Roth & Häusser, 2001) had no effect on IPSP amplification in PCs (Fig. 5) except for very small changes at hyperpolarized potentials (Fig. 6B left panel). The dependency of the amplitude and width of the model IPSPs on the modulation of  $\text{Ca}^{2+}$  currents and  $\text{Ca}^{2+}$ -activated  $\text{K}^+$  currents, respectively, predicts that a reduction of the extracellular  $\text{Ca}^{2+}$  concentration will decrease the amplitude and increase the width of somatically recorded IPSPs.

The dependency of attenuation of EPSPs on the synaptic location in cerebellar PCs was reported in a previous experimental and modeling work (Roth & Häusser, 2001). Those experiments and simulations focused on hyperpolarized membrane potentials, i.e.  $-70$  mV, and their model included only the  $I_h$  active channel. In the present study we compared only IPSPs elicited in spiny dendrites located in proximal or apical branches at membrane potentials corresponding to those observed *in vivo* (Loewenstein *et al.*, 2005).

### Functional implications

Inhibition sculpts the PC firing pattern in multiple ways. In the subthreshold domain inhibition is necessary to counteract the activation of dendritic voltage-gated channels during tonic firing. In fact, combined dynamic-clamp and modeling studies have shown that the total synaptic input to the PC should be net inhibitory to obtain the irregular firing pattern typically seen *in vivo* (Jaeger *et al.*, 1997; Jaeger & Bower, 1999). Inhibition also has a strong effect on the timing of spikes in the PC model (Jaeger *et al.*, 1997). This was confirmed in a slice study which showed that a single IPSP triggered by interneurons has direct control over the length of the PC interspike intervals (Häusser & Clark, 1997). The relation between the IPSP amplitude measured at the soma and the interspike interval prolongation is steep, suggesting a high sensitivity of the PC spike initiation to the inhibitory input.

The amplification of distal IPSPs and their constant width found in the present study seem more relevant to their effect on spike initiation. Irregularity of PC firing is more sensitive to the dendro-somatic balance in inhibitory conductance than in activation frequency (Fig. 8). In other words, the relative amplitude of dendritic vs. somatic IPSPs has a strong effect on spike initiation. This suggests that the range of the IPSP amplitudes recorded at the soma should be not too wide in order to limit the effect on the PC interspike intervals. Our findings show that the amplification mechanism fulfills these requirements. Indeed, the distribution of the IPSP amplitudes measured at the PC soma in experiments (Häusser & Clark, 1997) is similar to the ranges that we observed.

### Acknowledgements

This work was supported by FWO G.0097.04, EC QLRT-2000-02256 and HFSP RG0091/1999-B.

### Abbreviations

adPC, active dendrite Purkinje cell model; aPC, completely active PC model; b3s44, a distal dendritic branch of the PC model; b0s01, a proximal dendritic branch of the PC model; cIPSP, compound inhibitory postsynaptic potential; CV, coefficient of variation; K2, low voltage threshold  $Ca^{2+}$ -dependent  $K^+$  current; KC, BK-type  $Ca^{2+}$ -dependent  $K^+$  current; KM, noninactivating muscarinic  $K^+$  current; ldPC, leaky-dendrite passive PC model; P-type Ca, high threshold activated  $Ca^{2+}$  current; PC, Purkinje cell; pPC, completely passive PC model; SD, standard deviation; T-type Ca, low threshold activated  $Ca^{2+}$  current.

### References

Armstrong, D. & Rawson, J. (1979) Activity patterns of cerebellar cortical neurones and climbing fibre afferents in the awake cat. *J. Physiol. (Lond.)*, **289**, 425–448.  
Barbour, B. (1993) Synaptic currents evoked in Purkinje cells by stimulating individual granule cells. *Neuron*, **11**, 759–769.

Berger, T., Larkum, M.E. & Lüscher, H.-R. (2001) High  $I_h$  channel density in the distal apical dendrite of layer V pyramidal cells increases bidirectional attenuation of EPSPs. *J. Neurophysiol.*, **85**, 855–868.  
Bermader, O., Koch, C. & Douglas, R.J. (1994) Amplification and linearization of distal synaptic input to cortical pyramidal cells. *J. Neurophysiol.*, **72**, 2743–2753.  
Bower, J.M. & Beeman, D. (1998) *The Book of GENESIS: Exploring Realistic Neural Models with the GENeral NEural Simulation System*. TELOS, New York, NY.  
Chadderton, P.T., Margrie, T.W. & Häusser, M. (2004) Integration of quanta in cerebellar granule cells during sensory processing. *Nature*, **428**, 856–860.  
Cook, E.P. & Johnston, D. (1997) Active dendrites reduce location-dependent variability of synaptic input trains. *J. Neurophysiol.*, **78**, 2116–2128.  
Crepel, F. & Penit-Soria, J. (1986) Inward rectification and low-threshold calcium conductance in rat cerebellar Purkinje cells. An *in vitro* study. *J. Physiol. (Lond.)*, **372**, 1–23.  
Dean, I., Robertson, S.J. & Edwards, F.A. (2003) Serotonin drives a novel GABAergic synaptic current recorded in rat cerebellar Purkinje cells: a Lugaro cell to Purkinje cell synapse. *J. Neurosci.*, **23**, 4457–4469.  
De Schutter, E. (1998) Dendritic voltage and calcium-gated channels amplify the variability of postsynaptic responses in a Purkinje cell model. *J. Neurophysiol.*, **80**, 504–519.  
De Schutter, E. & Bower, J.M. (1994a) An active membrane model of the cerebellar Purkinje cell I. Simulation of current clamps in slice. *J. Neurophysiol.*, **71**, 375–400.  
De Schutter, E. & Bower, J.M. (1994b) An active membrane model of the cerebellar Purkinje cell II. Simulation of synaptic responses. *J. Neurophysiol.*, **71**, 401–419.  
De Schutter, E. & Bower, J.M. (1994c) Simulated responses of cerebellar Purkinje cells are independent of the dendritic location of granule cell synaptic inputs. *Proc. Natl Acad. Sci.*, **91**, 4736–4740.  
De Schutter, E. & Steuber, V. (2000) Modeling simple and complex active neurons. In De Schutter, E. (Ed.), *Computational Neuroscience: Realistic Modeling for Experimentalists*. CRC Press, Boca Raton, FL, pp. 233–258.  
Eccles, J.C. (1973) The cerebellum as a computer: patterns in space and time. *J. Physiol. (Lond.)*, **229**, 1–32.  
Eilers, J., Plant, T. & Konnerth, A. (1996) Localized calcium signalling and neuronal integration in cerebellar Purkinje neurones. *Cell Calcium*, **20**, 215–226.  
Harvey, R.J. & Napper, R.M.A. (1991) Quantitative studies of the mammalian cerebellum. *Prog. Neurobiol.*, **36**, 437–463.  
Häusser, M. & Clark, B.A. (1997) Tonic synaptic inhibition modulates neuronal output pattern and spatiotemporal synaptic integration. *Neuron*, **19**, 665–678.  
Isope, P. & Barbour, B. (2002) Properties of unitary granule cell → Purkinje cell synapses in adult rat cerebellar slices. *J. Neurosci.*, **22**, 9668–9678.  
Jack, J.J.B., Noble, D. & Tsien, R. (1975) *Electric Current Flow in Excitable Cells*. Clarendon Press, Oxford.  
Jaeger, D. & Bower, J.M. (1999) Synaptic control of spiking in cerebellar Purkinje cells: dynamic current clamp based on model conductances. *J. Neurosci.*, **19**, 6090–6101.  
Jaeger, D., De Schutter, E. & Bower, J.M. (1997) The role of synaptic and voltage-gated currents in the control of Purkinje cell spiking: a modeling study. *J. Neurosci.*, **17**, 91–106.  
Koch, C. & Segev, I. (2000) The role of single neurons in information processing. *Nat. Neurosci.*, **3**, 1171–1177.  
Kuhn, A., Aertsen, A. & Rotter, S. (2004) Neuronal integration of synaptic input in the fluctuation-driven regime. *J. Neurosci.*, **24**, 2345–2356.  
Loewenstein, Y., Mahon, S., Chadderton, P., Kitamura, K., Sompolinsky, H., Yarom, Y. & Häusser, M. (2005) Bistability of cerebellar Purkinje cells modulated by sensory stimulation. *Nat. Neurosci.*, **8**, 202–211.  
Maccacferri, G., Roberts, J.D.B., Szucs, P., Cottingham, C.A. & Somogyi, P. (2000) Cell surface domain specific postsynaptic currents evoked by identified GABAergic neurones in rat hippocampus *in vitro*. *J. Physiol. (Lond.)*, **524**, 91–116.  
Marsaglia, G. (1985) A current view of random number generators. In Billard, L. (Ed.), *Computer Science and Statistics: 16th Symposium on the Interface*. Elsevier Science Publishers, Atlanta, pp. 3–10.  
Miles, R., Tóth, K., Gulyás, A.I., Hájos, N. & Freund, T.F. (1996) Differences between somatic and dendritic inhibition in the hippocampus. *Neuron*, **16**, 815–823.  
Palay, S.L. & Chan-Palay, V. (1974) *Cerebellar Cortex*. Springer-Verlag, New York.

- Pouzat, C. & Hestrin, S. (1997) Developmental regulation of basket/stellate cell → Purkinje cell synapses in the cerebellum. *J. Neurosci.*, **17**, 9104–9112.
- Rall, W. (1970) Cable properties of dendrites and effects of synaptic location. In Andersen, P. & Jansen, J.K.S. (Eds), *Excitatory Synaptic Mechanisms*. Universitetsforlaget, Oslo, Norway, pp. 175–187.
- Rall, W. & Among-Snir, H. (1998) Cable theory of dendritic neurons. In Koch, C. & Segev, I. (Eds), *Methods in Neural Modeling: from Ions to Networks*. MIT Press, Cambridge, Massachusetts, pp. 27–92.
- Rapp, M., Segev, I. & Yarom, Y. (1994) Physiology, morphology and detailed passive models of guinea-pig cerebellar Purkinje cells. *J. Physiol. (Lond.)*, **474**, 101–118.
- Roth, A. & Häusser, M. (2001) Compartmental models of rat cerebellar Purkinje cells based on simultaneous somatic and dendritic patch-clamp recordings. *J. Physiol. (Lond.)*, **535**, 445–472.
- Solinas, S., Maex, R. & De Schutter, E. (2003) Synchronization of Purkinje cell pairs along the parallel fiber axis: a model. *Neurocomputing*, **52–54**, 97–102.
- Stuart, G., Spruston, N. & Häusser, M. (1999) *Dendrites*. Oxford University Press, Oxford.
- Sultan, F. & Bower, J.M. (1998) Quantitative Golgi study of the rat cerebellar molecular layer interneurons using principal component analysis. *J. Comp. Neurol.*, **393**, 353–373.
- Szilagyi, T. & De Schutter, E. (2004) Effects of variability in anatomical reconstruction techniques on models of synaptic integration by dendrites: a comparison of three Internet archives. *Eur. J. Neurosci.*, **19**, 1257–1266.
- Tabata, T., Haruki, S., Nakayama, H. & Kano, M. (2005) GABAergic activation of an inwardly rectifying K<sup>+</sup> current in mouse cerebellar Purkinje cells. *J. Physiol. (Lond.)*, **563**, 443–457.
- Williams, S.R. & Stuart, G. (2003a) Role of dendritic synapse location in the control of action potential output. *Trends Neurosci.*, **26**, 147–154.
- Williams, S.R. & Stuart, G.J. (2003b) Voltage- and site-dependent control of the somatic impact of dendritic IPSPs. *J. Neurosci.*, **23**, 7358–7367.
- Yoshida, T., Hashimoto, K., Zimmer, A., Maejima, T., Araishi, K. & Kano, M. (2002) The cannabinoid CB1 receptor mediates retrograde signals for depolarization-induced suppression of inhibition in cerebellar Purkinje cells. *J. Neurosci.*, **22**, 1690–1697.